

Parameters of 3D fractal dimension for a population of long spark discharges

Michał Molas and Marcin Szewczyk, *Senior Member, IEEE*

Abstract—Coordination insulation of transmission lines requires evaluation of voltage breakdown between live-to-live and live-to-earthed parts of the line conductors and the tower structure. Modeling work supports the design process, requiring experimental data for validation of the models to prove their relevance and accuracy. A fractal model has been proposed to embrace the statistical nature of the voltage breakdown in air. In this paper, we offer a method of providing parameters of electrical discharges that can be implemented in the process of fractal model validation. We propose a 3D fractal dimension calculation applied to a population of a set of electrical discharges of a given type. We report using this approach for long spark discharges generated with 3.4 MV lightning impulse and 2.3 MV switching impulse in controlled laboratory conditions for Sphere-Sphere and Sphere-Plane electrode systems. The reported results show the ability of the proposed approach to perform classification of the types of discharges, making it suitable for validation of simulation models, which was not feasible with the so far reported 2D calculations performed for individual discharges.

Index Terms—fractal model, air gap discharges, attachment probability, validation.

I. INTRODUCTION

Advancements in EHV (Extra High Voltage) and UHV (Ultra High Voltage) systems, which have been observed over the last years, require continuous development of insulation coordination studies of these systems [1]. Electrical strength of high-voltage insulation systems is one of the fundamental aspects related to the design and reliability of power system operation. The mechanism of development of electric discharges in these systems is not fully deterministic. In addition to such factors as the distribution of the electric field, space charges, or atmospheric conditions, several other random phenomena affect how the discharge is created. As reported in recent works, fractal modeling has been employed in lightning protection studies, e.g., in [2-6] to reproduce the randomness of the electrical channel propagation in space. The approach established for modeling lightning discharges can also be applied to long sparks, as demonstrated in [7], indicating the potential of using fractal models for studying long sparks. This particularly includes determining of the fifty-percent flashover

voltage, a key parameter in the design process of insulation systems. Development of modeling methods for long sparks requires to explore additional capabilities, to allow determining the discharge direction or estimating the probability of discharge occurrence in complex insulation systems, which may further enhance the effectiveness of insulation coordination studies. To advance the models, measurement data obtained from discharges of similar lengths to those existing in the actual systems are required. Data needed for development and validation of simulation models such as those reported in [2] can be then extracted based on the measurements performed in laboratory-controlled conditions for long spark discharges in air, as reported in this paper.

The key parameter of the fractal model is a fractal dimension [8, 9], allowing a quantitative characterization of the discharge trajectory using only one parameter. The fractal dimension is a parameter depending on the type of the discharge; therefore, it can be utilized to compare discharges occurring under various conditions. This was recently reported in [10] for HVDC transmission lines, and in [11] for rotating wind turbines (also in earlier works [12, 13]). The classification of types of discharges can be used to verify simulation models of voltage discharges such as those reported in [2, 3]. For example, for small surface discharges of several millimeters developing in SF₆ gas, the fractal dimension is 1.7 [9], while in the case of large scale discharges: 1.34 ± 0.05 [12].

For long spark discharges, the fractal dimension analysis was reported in [14] and [15], where the determined values of the fractal dimension were given, and the method of preparing the measurement data was described. In [14], measurements of 18 discharges with an average length of approximately 500 mm were carried out. Pictures of sparks taken simultaneously by three cameras were used as input data, which allowed to obtain a total of 54 pictures. The tests were performed for both polarities of the voltage impulses (without defining the shape of the impulses) and different values of the breakdown voltages, however, not exceeding 100 kV. Higher voltages were used in [15], where the fractal dimension was determined for the discharges generated in the 6 m spark gap. For the fractal dimension analysis in [15], images recorded by a high-speed camera and two additional cameras were used. The research involved calculations of the

Manuscript received ...; revised ...; accepted Date of publication ...; date of current version

M. Molas is with Institute of Power Engineering, Mory 8 St., Warsaw, 01-330, Poland (e-mail: michal.molas@ien.com.pl). M. Szewczyk is with Warsaw

University of Technology, Faculty of Electrical Engineering, Electrical Power Engineering Institute, Division of Power Apparatus, Protection and Control, Koszykowa 75 St, 00-662, Warszawa, Poland (e-mail: marcin.szewczyk@pw.edu.pl).

fractal dimension for the switching and lightning impulses of both polarities, which showed that the fractal dimension depends on the type of discharge (switching or lightning) and its polarity.

In all the works mentioned above, the fractal dimension was calculated for individual discharges in two-dimensional (2D) space. The discharges, however, are spatial objects; therefore, this paper defines the fractal dimension in three-dimensional (3D) space, both for individual discharges and their population. The results reported in this paper are then analyzed in terms of the feasibility of using them for the classification of discharges, which enables the validation of long spark simulation models based on the data reported.

The tests were carried out for long spark discharges, for which it is feasible to determine the spatial trajectory of the discharge. Moreover, the long spark is characterized by a relatively small number of branches, which reduces inaccuracy associated with the reconstruction of the discharge channel. Conducting tests in laboratory-controlled conditions allows for accurate observation of the phenomenon, unlike in the case of lightning discharges, where spatial observation of the discharge is much more challenging due to the size and random occurrence.

discussion of the results, and Section VI gives general conclusions.

The analyses are reported for 1080 images of long spark discharges recorded in 12 configurations (45 discharges for each configuration): for switching and lightning impulses (further referred to as SI and LI, respectively), with positive and negative polarities (further referred to as + and -, respectively), in a sphere-sphere and sphere-plate electrode system arrangements (further referred to as S-S and S-P, respectively) and distances 3.3 m and 5.5 m.

II. FRACTAL DIMENSION OF LONG SPARK DISCHARGES

A. Box Counting Method

In this paper, fractal dimension was calculated with the use of the Box Counting Method [14]. This method can be used for various geometric structures, including those that are not fractals (also without fractal features, in particular self-similarity), and allows for determining the fractal dimension of both 2D and 3D objects.

The fractal dimension $D_b(F)$ is defined by the formula [15]:

$$D_b(F) = \lim_{\delta \rightarrow 0} \frac{\log N_\delta}{\log(1/\delta)}, \quad (1)$$

where N_δ is the smallest number of cubes with an edge δ that is needed to cover the object under consideration completely.

Fig. 1a-c shows a method of covering the discharge channel (SI+, S-S, 5.5m) with boxes of different dimensions δ . It graphically illustrates the relationship between the number of boxes N_δ needed to fully cover the discharge channel and their size δ (as a result of reducing the size of the boxes δ , their number N_δ increases).

In practice, it is not feasible to determine the fractal dimension following the formula (1) because the concept of the limit can only be applied for abstract objects. Therefore, the formula (1) transforms into a form that allows the calculation of the fractal dimension of the real object. The relationship (1) suggests a relationship of the type $N_\delta = c_\delta \cdot \delta^{-D_b(F)}$ [16], which can be written as:

$$\log N_\delta = D_b(F) \cdot \log(1/\delta) + \log(c_\delta), \quad (2)$$

where $\log(c_\delta)$ is a constant term. Determination of the fractal dimension according to formula (2) comes down to the determination of the function describing the relationship between the dimensions of the boxes δ and their minimal number N_δ that is necessary to cover the entire object. Knowing this relationship, the fractal dimension $D_b(F)$ is determined by calculating the slope of the regression line on the logarithmic plot of the number of boxes N_δ over their size δ .

Fig. 1d shows the relationship between the quantities N_δ and δ for determining the fractal dimension. Selected points of this relationship are marked with black dots, and the red dots are the points determined for the boxes shown in Fig. 1a-c. On their basis, a linear regression curve was drawn (see Fig. 1d), the slope of which is, according to equation (2), the fractal dimension $D_b(F)$.

The fractal dimension is calculated using the same dependencies for 2D and 3D objects. The difference is that for two-dimensional objects, the image is covered with squares, and for three-dimensional objects – with cubes.

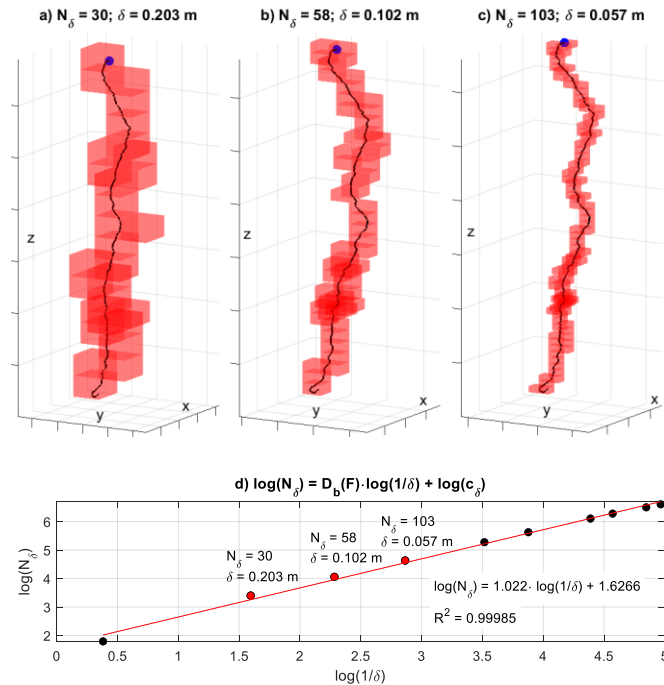


Fig. 1. Applying box-counting method to a 3D discharge channel recorded in SI+/S-S/5.5m configuration. Relationship between number of boxes N_δ needed to fully cover the discharge channel and their size δ (a-c). Relationship between N_δ i δ used to determine the fractal dimension shown with dots (d). According to (2), the fractal dimension is the slope of a linear regression curve drawn from dots (d). The red dots in (b) represent the parameters N_k and δ

The paper is organized as follows. Section II introduces the fractal dimension concept and box-counting method used in this paper for the fractal dimension calculation. Evaluation of calculation errors of the method is given by comparing the calculated results with analytically known results for 2D and 3D fractals. Section III presents the measurement test setup and test procedure. Section IV reports on test results for the fractal dimension of individual discharges in 2D and 3D and the 3D fractal dimension of spark population. Section V offers a detailed

B. Calculation errors

The measurement error of the fractal dimension was estimated based on the analysis of objects with a known fractal dimension. For this purpose, four fractals were used: Sierpinski Triangle and Sierpinski Carpet representing two-dimensional objects, and Sierpinski Tetrahedron and Menger Sponge representing three-dimensional objects. These fractals were generated numerically; therefore, similarly to the electric discharge channel, they were defined by a set of points with a given resolution (in the case of the discharge channel, the resolution with which the trajectory is determined results from the resolution of the recorded photos showing the long spark).

Fig. 2 and Fig. 3 show the used fractals (top) together with the corresponding linear regression functions (bottom) obtained according to the formula (2) as introduced in Fig. 1. In all cases a very good fit of the approximating function was obtained, which is demonstrated by the coefficient of determination R^2 , the value of which was in each case higher than 0.999.

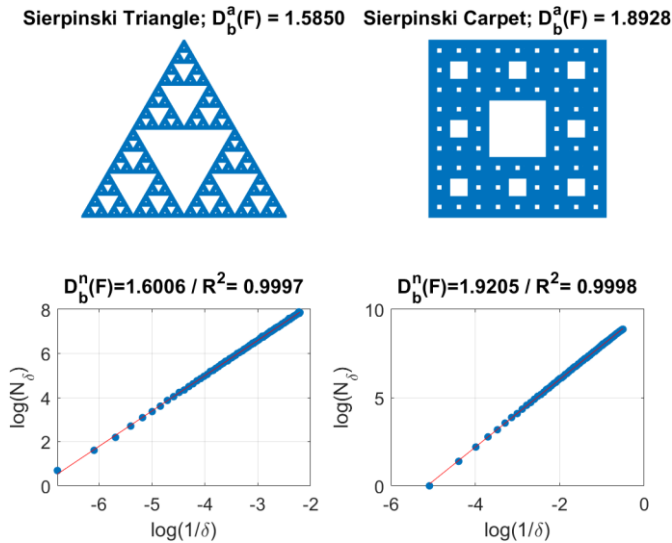


Fig. 2. Sierpinski Triangle (left) and Sierpinski Carpet (right) representing **two-dimensional** objects (top) with analytically known fractal dimensions $D_b^a(F)$. Corresponding linear regression curves (bottom) based on which the fractal dimensions $D_b^n(F)$ were determined numerically with the coefficient of determination R^2 .

Table I shows the results of the calculations performed for the four fractals shown in Fig. 2 and Fig. 3, together with the values of the calculation errors. It was assumed that the measurement error is equal to the relative difference between the numerically calculated fractal dimension $D_b^n(F)$ and analytically $D_b^a(F)$ (exact value), expressed as a percentage of the analytically calculated value $D_b^a(F)$. The calculations presented in Table I show that the measurement error increases with the increase of the fractal dimension itself, which applies to both two-dimensional and three-dimensional objects.

For the purposes of this study, it was assumed that the error in determining the fractal dimension is 1.4% for two-dimensional objects and 2.5% for three-dimensional objects.

The measurement uncertainty of the peak voltage applied for discharge initiation was estimated as $\pm 0.97\%$ for lightning impulse voltages and $\pm 0.86\%$ for switching impulse voltages.

Sierpinski Tetrahedron; $D_b^a(F) = 2.0000$ Menger Sponge; $D_b^a(F) = 2.7268$

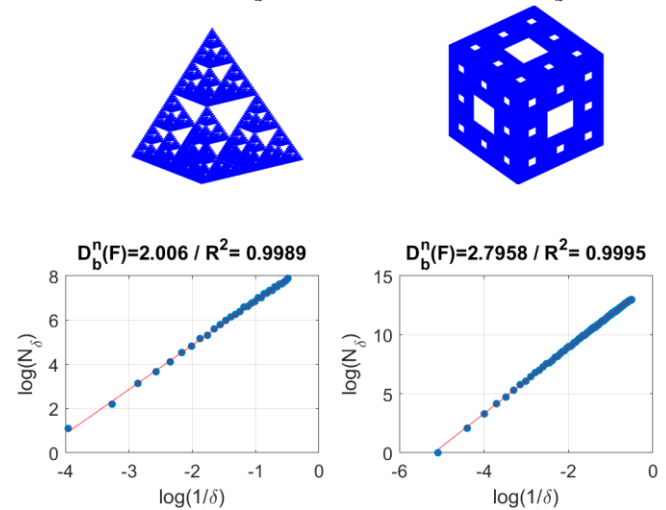


Fig. 3. Sierpinski Tetrahedron (left) and Menger Sponge (right) representing **three-dimensional** objects (top) with analytically known fractal dimensions $D_b^a(F)$. Corresponding linear regression curves (bottom) based on which the fractal dimensions $D_b^n(F)$ were determined numerically with the coefficient of determination R^2 .

III. MEASUREMENT TEST SET-UP AND TEST PROCEDURE

A. Measurement test set-up

There are no published data on how the fractal dimension is influenced by the system in which the discharges develop. Specifically, no published data exist on whether the fractal dimension of discharges occurring between the line and the structure differs from that of discharges occurring between, for example, arcing horns of insulator strings. To investigate this phenomenon, we studied voltage breakdowns in two electrode configurations. The test system was a spark gap with a sphere-sphere (S-S) and sphere-plate (S-P) geometry, as shown in Fig. 4. These systems are typical high-voltage testing systems, hence measurements performed in them allow to compare the obtained results with the results widely described in the literature, typically obtained in sphere-sphere and rod-plate set-ups. In our test set-up the sphere was used instead of the typically used rod electrode because the sphere's geometry is well-defined, which is more appropriate for simulation studies. The use of universal model systems, such as the rod-structure and conductor-structure, is a common approach in insulation coordination studies of high-voltage overhead lines [17].

The spark gap was connected to a Marx impulse voltage generator (375 kJ, 25 steps), applying switching impulses 250/2500 us/us (SI) with a crest voltage up to 2.3 MV and lightning impulses 1.2/50 us/us (LI) with crest voltage up to 3.4 MV. The impulses were generated with positive (+) and negative (-) polarity. These impulse voltages comply with the principles applied in insulation coordination. According to the currently adopted classification (see Table 1 in [17]), there are three types of transient overvoltages: Slow-Front, Fast-Front, and Very-Fast-Front. For systems such as overhead lines, considerations regarding electrical strength focus on the first two types of overvoltages: Slow-Front and Fast-Front. For testing the impact of these types of overvoltages on dielectric strength, standardized impulse voltages are used, respectively, switching impulse and lightning impulse. In our case, the distance between the electrodes was 3.3 m for both

types of test voltages, electrode configurations, and polarization. For impulses with positive polarization, measurements were additionally made for both types of impulses and both configurations of the electrodes at an increased distance of 5.5 m.

The impulse voltages were generated with a 25-stage Marx generator, featuring impulse energy of 375 kJ and a maximum voltage of 4.5 MV for lightning and 2.8 MV for switching impulses (in our study, the crest voltages of 3.8 MV and 2.7 MV were used to generate lightning and switching impulses, respectively). A Capacitive Impulse Voltage Divider CRS 4500 kV with a ratio of $v = 3150$ was used for measuring voltage with the output signal sent via a 50-m long coaxial cable with a surge impedance of 75Ω to a Dr Strauss TR-AS 200-14 4-channel digital voltage recorder with a maximum input voltage of 2 kV and 14 bit resolution. The impulse voltages were shaped by selection of the Marx generator elements, namely a damping resistor R_t and a discharge resistor R_r ($R_t = 25 \times 1.17 = 29.25 \text{ k}\Omega$ and $R_r = 25 \times 4.59 = 114.75 \text{ k}\Omega$ for switching impulses, $R_t = 25 \cdot 18 = 450 \Omega$ and $R_r = 25 \cdot 89 = 2225 \Omega$ for lightning impulses). This allowed to obtain the impulse shape parameters defined in [18] by the time-to-peak (T_p) and the time-to-half-value (T_2) for switching impulses and front-time (T_1) and the time-to-half-value (T_2) for lightning impulses. The capacitance per stage of the Marx generator C_g and the high voltage capacitance C_{HV} of the voltage divider were constant during testing and were, respectively: $C_g = 0.75/25 = 0.03 \mu\text{F}$ and $C_{HV} = 600 \text{ pF}$. Further details of the measuring system are reported in [19].

TABLE I
CALCULATION ERRORS FOR NUMERICAL $D_b^a(F)$ RELATIVE TO ANALYTICAL $D_b^a(F)$ FRACTAL DIMENSION, AS SHOWN IN FIG. 2 AND FIG. 3

Fractal name	Fractal dimension analytical, $D_b^a(F)$	Fractal dimension numerical, $D_b^a(F)$	Error
Sierpinski Triangle (2D)	1.5850	1.6006	1.0%
Sierpinski Carpet (2D)	1.8928	1.9205	1.4%
Sierpinski tetrahedron (3D)	2.0000	2.0060	0.3%
Menger Sponge (3D)	2.7268	2.7958	2.5%

Examples of recorded waveforms of the switching and lightning impulse test voltages are shown in Fig. 5. The spark initiation was observed at the impulse front for switching impulses (see Fig. 5-left) and at the tail for lightning impulses (see Fig. 5-right). The values of breakdown voltages were assumed as the peak voltage values recorded during the discharges. The voltage was recorded with a digital voltage recorder with a maximum input voltage of 2 kV and 14-bit resolution. For the switching impulses, 50 MS/s sampling frequency was used, while 200 MS/s for the lightning impulses.

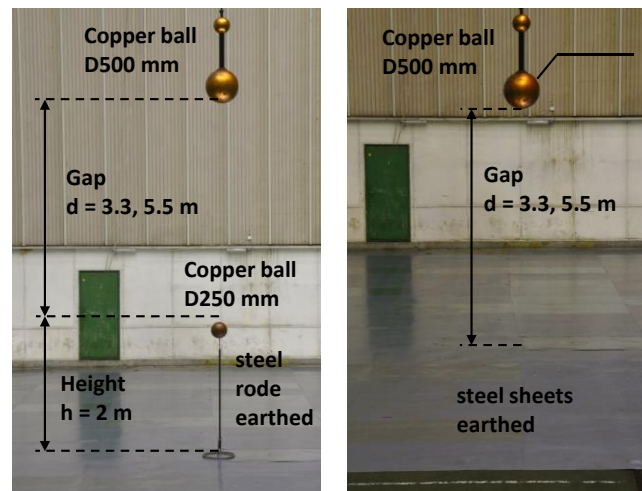


Fig. 4. Electrode configurations used in testing: (a) sphere-sphere (S-S) with 500 mm diameter copper ball at high voltage and 250 mm diameter copper ball on the top of the steel rod earthed; (b) sphere-plane (S-P) with same copper ball at high voltage and steel sheets earthed measuring 17 m x 11 m. Distance between electrodes: $d = 3.3 \text{ m}, 5.5 \text{ m}$.

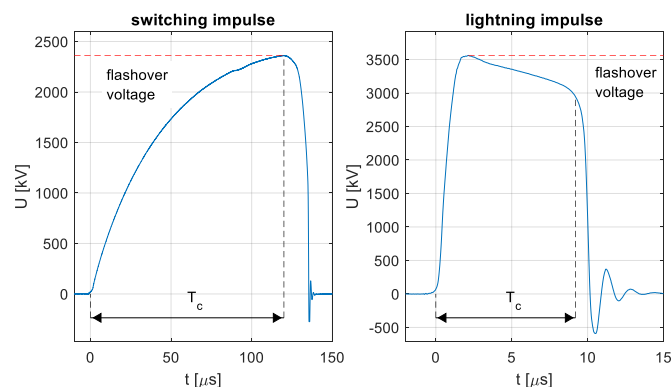


Fig. 5. Examples of switching (left) and lightning (right) impulses recorded during testing. Breakdown voltages are, respectively, 2.36 MV and 3.56 MV; impulse chopping typically occurred, respectively, in the front and at the tail of the impulses; T_c – time-to-chopping.

B. Test procedure

The spark trajectory was recorded with two synchronized Nikon D750 cameras placed perpendicularly to each other to record the discharges projection onto the X plane and Y plane (see Fig. 6a-b). The cameras were placed in metal housings for protection and shielding against discharges. A 40 meters fiber link was used to synchronize and connect the cameras with the control and acquisition unit. The measurement results were a set of photos recorded simultaneously for two observed planes, based on which the 2D trajectories were determined (see Fig. 6c-d).

Table II shows the atmospheric conditions during the measurements. The breakdown voltage values were converted to normal atmospheric conditions: $t_0 = 20 \text{ degC}$, $p_0 = 1013 \text{ hPa}$, $h_0 = 11 \text{ g/m}^3$ according to a procedure described in [18].

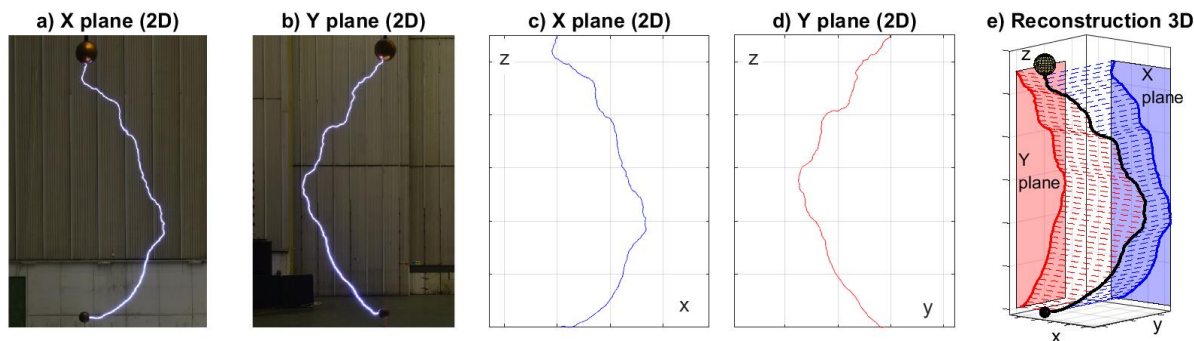


Fig. 6. Discharge channel reconstruction: photographs (a,b) and 2D trajectories (c,d) in X plane (a,c) and Y plane (b,d). Reconstructed 3D channel for SI+/S-S/5.5m configuration (e).

TABLE II
ATMOSPHERIC CONDITIONS DURING MEASUREMENTS;
TEMPERATURE t , HUMIDITY R , PRESSURE p

	t [°C]	R [%]	p [hPa]
mean	7.6	80	1002
min	6.8	70	999
max	9.1	88	1013

For determining the discharge trajectory, it was assumed that it corresponds to the central line of the recorded discharge channel. The Delaunay triangulation method [20, 21] was used to determine the central line. From the geometric point of view, the photos of the discharge channel and the photos of the objects analyzed in [20, 21] are very similar to each other, which allows the adaptation of already existing and validated method. The division of the discharge channel into segments was performed using image analysis methods and built-in functions of the Matlab package. An example result is shown in Fig. 7.

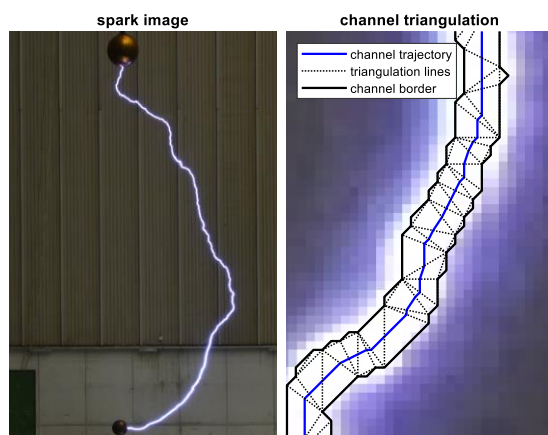


Fig. 7. An example of obtaining the discharge trajectory as the central line determined using the Delaunay method.

Then, from the 2D trajectories, the 3D trajectory was reconstructed based on methods described in [22, 23] (see Fig. 6e). The fractal dimension was calculated for both 2D and 3D

trajectories. Fig. 6 shows examples of photos recorded (see Fig. 6a-b) along with the 2D trajectory determined on their basis in the X and Y planes (see Fig. 6c-d) and the 3D trajectory reconstructed on this basis (see Fig. 6e). In Fig. 6c-e, the discharge channel is shown as a trajectory line.

The value of the fractal dimension is influenced by the thickness of the discharge channel. The channel's thickness depends on the discharge current value and the cameras' sensitivity. The impact of the discharge channel thickness was eliminated by converting the image of the discharge channel into a trajectory defined by a set of points connected by lines. Such an object has no thickness, and the fractal dimension depends solely on the shape of the trajectory.

IV. TEST RESULTS AND DISCUSSION

A. Fractal dimension in 2D for individual sparks

The fractal dimension $D_b(F)$ was determined for each of the 45 discharges recorded in each of the 12 configurations of the measuring system (540 discharges recorded in total). Then, for each configuration of the measurement system, the average value of the fractal dimension, $D_b(F)_{\text{mean}}$, and its standard deviation σ_{D_b} were calculated, providing the fractal dimension characteristic for a given configuration of the measurement system. In each case, the calculations were performed twice because the discharge trajectory was simultaneously recorded in two planes perpendicular to each other (X and Y planes, see Fig. 6).

Fig. 8-left shows the results for 2D calculations. Top figure in Fig. 8-left shows the fractal dimension $D_b(F)$ for a population of $N = 45$ discharges recorded in the selected system (SI+/S-P/3.3m). The bottom figure in Fig. 8-left shows the mean values of the fractal dimension $D_b(F)_{\text{mean}}$ (as shown with the dashed line in top Fig. 8-left) and standard deviations σ_{D_b} for all sparks recorded in each of the 12 measurement system configurations. The results of $D_b(F)$ and $D_b(F)_{\text{mean}}$ are shown in Fig. 8-left for sparks recorded in two planes: X plane (in blue) and Y plane (in red).

The measurement results shown in Fig. 8-bottom are summarized in Table III. Apart from the average values of the fractal dimension $D_b(F)_{\text{mean}}$, Table III also shows the values of the standard deviation σ_{D_b} , based on which it is feasible to assess the dependence of the fractal dimension on the type of the measurement system.

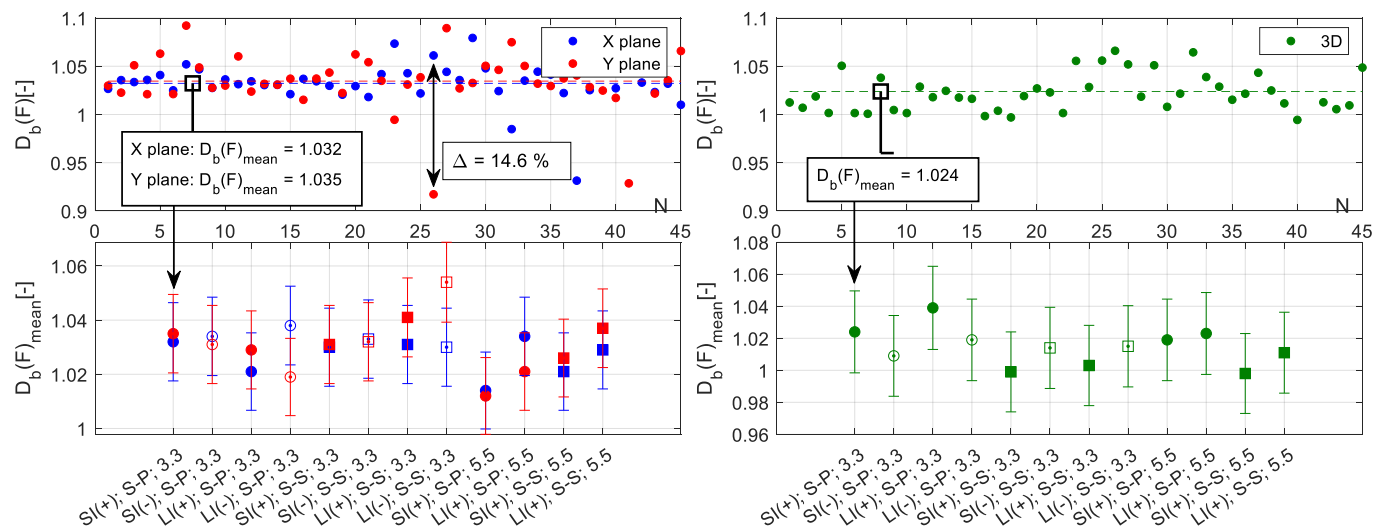


Fig. 8. Measurement results of the fractal dimension $D_b(F)$ for selected configuration of the measurement system SI+/S-P/3.3m (top). Mean values $D_b(F)_{\text{mean}}$ and standard deviations σ_{D_b} for all 12 configurations of the measurement system (bottom). Calculations for 2D (left) and 3D (right) trajectories. The red and blue in the left figures denote calculations for X plane 2D and Y plane 2D, respectively. Dashed lines in the top figures denote mean values $D_b(F)_{\text{mean}}$ shown in the bottom figures for SI+/S-P/3.3m configuration. Circles denote S-P, squares denote S-S, solid marks denote “+”, empty marks denote “-”.

TABLE III

2D RESULTS: MEAN VALUES $D_b(F)_{\text{MEAN}}$ AND STANDARD DEVIATIONS σ_{D_b} OF THE FRACTAL DIMENSION FOR INDIVIDUAL CONFIGURATIONS OF THE MEASURING SYSTEM, AS SHOWN IN FIG. 8 LEFT-BOTTOM

Impulse ¹	d [m]	Electrodes ²	X plane		Y plane	
			$D_b(F)_{\text{mean}}$	σ_{D_b}	$D_b(F)_{\text{mean}}$	σ_{D_b}
SI (+)	3.3	S—P	1.032	0.022	1.035	0.032
SI (-)	3.3	S—P	1.034	0.030	1.031	0.023
LI (+)	3.3	S—P	1.021	0.065	1.029	0.056
LI (-)	3.3	S—P	1.038	0.051	1.019	0.051
SI (+)	3.3	S—S	1.030	0.022	1.031	0.012
SI (-)	3.3	S—S	1.033	0.037	1.032	0.030
LI (+)	3.3	S—S	1.031	0.012	1.041	0.018
LI (-)	3.3	S—S	1.030	0.044	1.054	0.042
SI (+)	5.5	S—P	1.014	0.045	1.012	0.053
LI (+)	5.5	S—P	1.034	0.049	1.021	0.039
SI (+)	5.5	S—S	1.021	0.013	1.026	0.011
LI (+)	5.5	S—S	1.029	0.034	1.037	0.038

¹SI/LI—switching/lightning impulse, +/- —positive/negative polarity; ²S—sphere electrode, P—plane electrode.

TABLE IV

3D RESULTS: MEAN VALUES $D_b(F)_{\text{MEAN}}$ AND STANDARD DEVIATIONS σ_{D_b} OF THE FRACTAL DIMENSION FOR INDIVIDUAL CONFIGURATIONS OF THE MEASURING SYSTEM, AS SHOWN IN FIG. 8 RIGHT-BOTTOM

Impulse ₁	d [m]	Electrodes ₂	$D_b(F)_{\text{mean}}$	σ_{D_b}
SI (+)	3.3	S—P	1.024	0.021
SI (-)	3.3	S—P	1.009	0.021
LI (+)	3.3	S—P	1.039	0.031
LI (-)	3.3	S—P	1.019	0.018
SI (+)	3.3	S—S	0.999	0.017
SI (-)	3.3	S—S	1.014	0.019
LI (+)	3.3	S—S	1.003	0.013
LI (-)	3.3	S—S	1.015	0.027
SI (+)	5.5	S—P	1.019	0.032
LI (+)	5.5	S—P	1.023	0.027
SI (+)	5.5	S—S	0.998	0.016
LI (+)	5.5	S—S	1.011	0.014

¹SI/LI—switching/lightning impulse, +/- —positive/negative polarity; ²S—sphere electrode, P—plane electrode.

Considering the results in Table III, the fractal dimension for the long spark presented as a discharge trajectory in 2D space is practically constant. This confirms the observations presented in [14], where the differences in the fractal dimension between the discharges with positive and negative polarity are within the estimated statistical error of ± 0.02 . Additionally, the fractal dimension does not significantly depend on the direction of observation. The differences between the mean values $D_b(F)_{\text{mean}}$ calculated for the X plane and Y plane (see Fig. 6) are less than the measurement error (1.4%, see Section II.B). However, considering the discharges individually, for some sparks, the fractal dimension $D_b(F)$ depends on the direction of observation, as illustrated, for example, by the relative difference $\Delta = 14.6\%$ (see the top figure in Fig. 8-left) between the sparks observed in the X plane and Y plane, which exceeds the measurement error by more than ten times (1.4%, see Section II.B). A similar observation was reported in [15], where, therefore, attention was drawn to the need to analyze the fractal dimension in three-dimensional space, which

was supposed to reduce errors resulting from the choice of the direction of the discharge observation.

B. Fractal dimension in 3D for individual sparks

The fractal dimension of the discharge channel in three-dimensional space was calculated the same way as it was for the two-dimensional system. In the first step, the value of $D_b(F)$ was calculated for each spark. Then the average value $D_b(F)_{\text{mean}}$ was determined, characteristic for the given configuration of the measuring system. These values are shown in Fig. 8-right and summarized in Table IV in the same way as to the description given above for Fig. 8-left and Table III, respectively.

Based on the data presented in Fig. 8-right and Table IV, the fractal dimension in the 3D space is characterized by even less differentiation between individual configurations of the measurement system than in the case of the 2D space. Within one configuration of the measurement system, the fractal dimension has much smaller values of the standard deviation (the standard deviation of the fractal dimension in 3D is smaller by about 55-

60% than in the case of the 2D). However, when the results obtained in different configurations are compared, it is noticeable that they all fall within the assumed measurement error (amounting to 2.5%, see Section II.B).

Summing up, the fractal dimension determined as the mean value of the fractal dimensions of the series of sparks obtained in a given configuration does not indicate the differences between the measuring systems. It can be therefore concluded that the fractal dimension of the discharge channel defined by the three-dimensional long spark trajectory is approximately constant and does not depend on the type and polarity of the voltage, as well as the type and distance of the electrodes; and its value is 1.015 ± 0.025 .

C. 3D fractal dimension of spark population

When calculating the fractal dimension as the average of the values determined for single sparks, it is assumed that the discharges for a given configuration of the measurement system form a population. Fig. 9 shows an example of two sets of discharges recorded for switching impulses (shown in Fig. 9a) and lightning impulses (shown in Fig. 9b). In both cases, the electrodes were configured in the S-S system and formed a spark gap 5.5 m long. These sets were created as a result of overlapping the trajectories of all 45 sparks recorded in a given measurement system configuration.

Comparing the two populations, significant differences can be seen in the shape of their images. In the case of sparks resulting from switching impulses (see Fig. 9a), the discharge channels occupy a much larger space than the sparks resulting from the lightning impulses (see Fig. 9b), where the discharge trajectories run much closer to each other, creating a seemingly compact structure.

Calculating the fractal dimension of the entire population of discharges is performed the same way as for a single spark. Fig. 9c-d show the set of discharges from Figs. 9a-b and the corresponding image, which depict the boxes superimposed on the examined structure of the discharges. In this case, only one value of fractal dimension is determined for the entire population of sparks registered in each configuration of the measuring system. The presented approach does not require the

calculation of the mean value of the fractal dimension (as it was in the case of calculations for 2D and 3D individual spark discharges as discussed in Sections IV.A and IV.B), which reduces the impact of statistical errors resulting from a large dispersion of results for individual sparks.

The calculated fractal dimension of the spark population is very much dependent on the number of discharges making up the population. Fig. 10-left shows the effect of the number of discharges N on the fractal dimension $D_b(F)$. It is characteristic that regardless of the type of discharge, polarity, type of electrodes, and the length of the spark gap, the fractal dimension of the discharge population increases with the population size N increase. The fractal dimension shown in Fig. 10-left can be approximated by the logarithmic function, which for an example measuring system SI+/S-S/5.5m takes the form $D_b(F) = 0.2625 \cdot \log(N) + 0.921$ ($R^2 = 0.9807$). This is consistent with the intuition that the impact of successive sparks added to the population decreases as the population increases, and this is because each subsequent discharge changes the shape of the entire structure to a lesser degree.

In this paper, it was assumed that the fractal dimension describing a given configuration of the measurement system is calculated for a population of 45 discharges (the number of discharges recorded for each configuration of the system). The results of the fractal dimension calculations of the population of all 45 sparks in each measurement system are shown in Fig. 10-right and summarized in Table V.

Contrary to the previously discussed 2D (see Section IV.A) and 3D (see Section IV.B) approaches, in which the discharges were considered individually, and the fractal dimension $D_b(F)$ was defined as the mean value $D_b(F)_{\text{mean}}$ and standard deviation σ_{D_b} , the approach in which the entire population is analyzed is characterized by a greater dispersion of the results of the fractal dimension $D_b(F)$ between measurement configurations. Fig. 10-right shows that the differences of the fractal dimensions for different types of configurations are greater than the measurement error (assumed as 2.5%, see Section II.B).

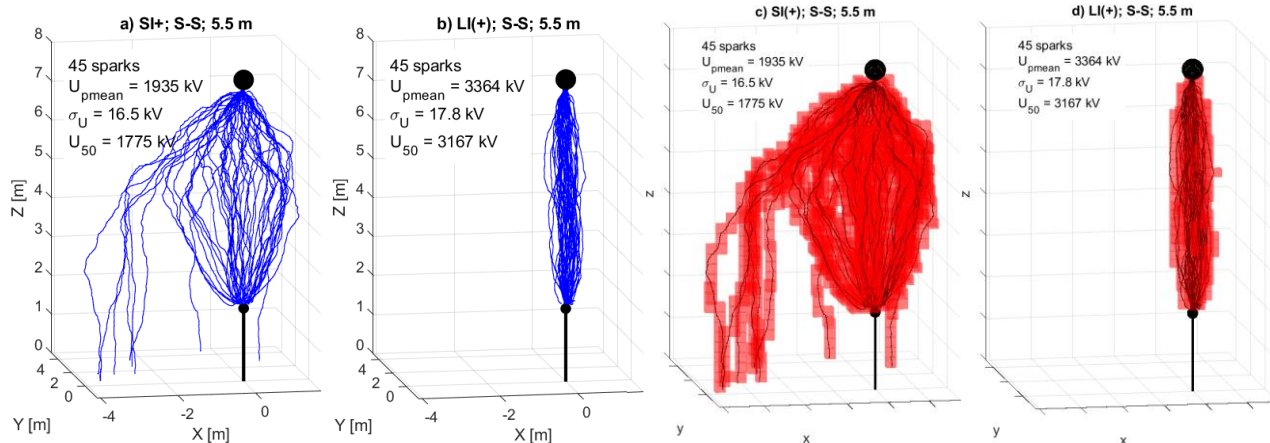


Fig. 9. Comparison of the spark population trajectory for SI+ (a, c) and LI+ (b, d). Recorded sparks (a, b) with plotted cubes of the Box Counting Method to calculate the fractal dimension (c, d). In both cases (SI+, LI+), the measuring electrodes were configured in the sphere-sphere (S-S) system with a spark gap of 5.5 m. $U_{p\text{mean}}$ and σ_U – mean value and standard deviation of the flashover voltage distribution, U_{50} – 50% flashover voltage.

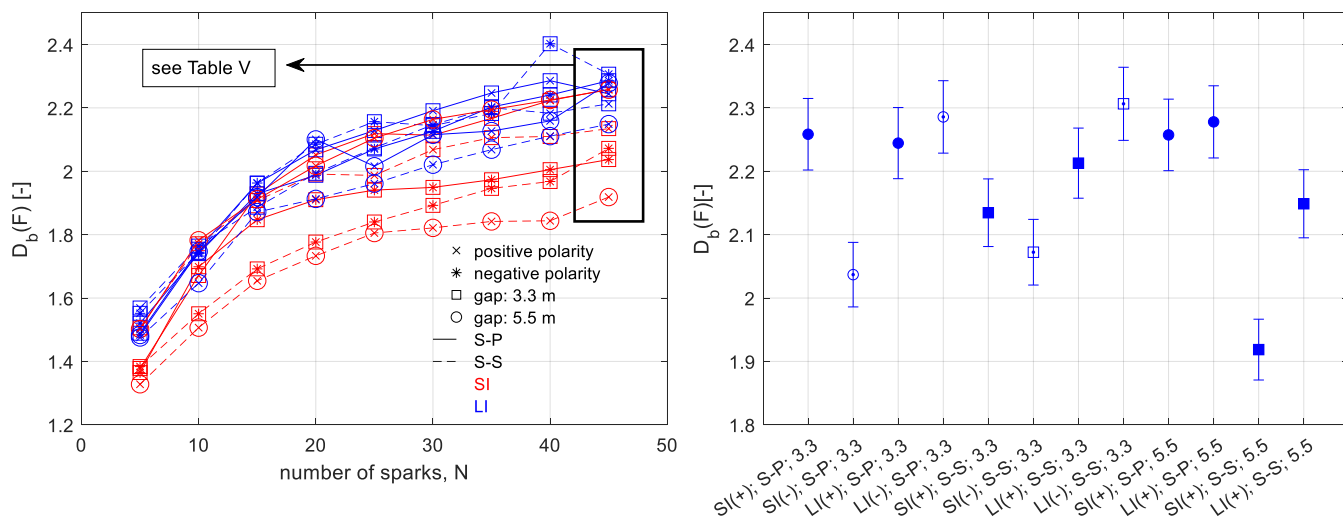


Fig. 10. Results of 3D calculations of the fractal dimension $D_b(F)$ for the population of sparks for all configurations of the measurement system: a) impact of the population size on the fractal dimension (N – number of sparks in the population), b) values of the fractal dimension $D_b(F)$ for all configurations with an error 2.5% estimated in Section II for three-dimensional objects. Circles denote S-P, squares denote S-S, solid marks denote “+”, empty marks denote “-”.

V. DISCUSSION

Results presented in Table V show that the value of the fractal dimension of the discharge population depends on the type and polarity of the discharge, as well as on the geometry of the system in which the discharge was initiated. This is contrary to the results of average values and their standard deviations obtained for individual sparks, as summarized in Table III and Table IV.

Regardless of the type of electrodes, in the case of negative polarity, the fractal dimension of the lightning impulses population is greater than that of switching impulses, and the difference is 11%. A similar regularity also occurs in the case of positive polarity. At the same time, the observed differences are smaller (approximately 3.5%) and can be observed only in the S-S system (in the S-P system, the measured differences are smaller than the measurement error 2.5%).

TABLE V
3D FRACTAL DIMENSION $D_b(F)$ FOR POPULATION, FOR ALL CONFIGURATIONS OF THE MEASURING SYSTEM, AS SHOWN IN FIG. 9-RIGHT

Impulse ¹	d [m]	Electrodes ²	$D_b(F)$
SI (+)	3.3	S—P	2.258
SI (-)	3.3	S—P	2.037
LI (+)	3.3	S—P	2.244
LI (-)	3.3	S—P	2.286
SI (+)	3.3	S—S	2.135
SI (-)	3.3	S—S	2.072
LI (+)	3.3	S—S	2.213
LI (-)	3.3	S—S	2.306
SI (+)	5.5	S—P	2.257
LI (+)	5.5	S—P	2.278
SI (+)	5.5	S—S	1.919
LI (+)	5.5	S—S	2.149

¹SI/LI—switching/lightning impulse, +/- —positive/negative polarity;
²S—sphere electrode, P—plane electrode.

Comparing the discharges of the same type, for switching impulses, the fractal dimension of discharges with positive polarity is greater than for negative polarity. The differences are more visible in the S-P system (differences at 10%) than in the

S-S system (differences at 3%). However, in the case of lightning impulses, the tendency is the opposite. The fractal dimension of the LI+ discharges is approximately 4% smaller than for the LI- discharges (this observation applies only to the S-S system because, in the S-P system, the measured differences are again smaller than the measurement error 2.5%).

Regardless of the type and polarity of the discharge, the differentiation of the fractal dimension value is greater in the S-S system than in the S-P system. It is evident in the case of discharges with a length exceeding 5.5 m, for which the differences between the SI and LI discharges exceed 11% in the S-S system. In contrast, for the S-P system, they are approximately 1%, which is less than the measurement error 2.5%.

Based on the above discussed results, it can be concluded that the fractal dimension of the discharges population can be used for partial classification of discharges. Knowing the polarity of the discharge, one can determine its type based on the fractal dimension. Similarly, knowing the discharge type makes it feasible to determine its polarity. With this respect, the fractal dimension of the population can be used to evaluate the results of simulation studies and validate simulation models.

VI. CONCLUSIONS

This paper reports on the fractal dimension of long laboratory spark discharges analyzed for individual spark trajectories in 2D and 3D and for the whole 3D population. The results are based on the measured long spark discharges in 12 high voltage laboratory test set-up arrangements at voltage levels of up to 4.5 MV and distances between electrodes up to 5.5 m.

As the long spark is a spatial object, the paper introduces an approach to analyzing the fractal dimension of long spark discharges based on a three-dimensional analysis. Instead of analyzing each spark individually, simultaneous analysis of all sparks within a given population is proposed to calculate the fractal dimension of the entire population of discharges. The fractal dimension values obtained thanks to the proposed method enable the classification of the type (lightning impulse LI or switching impulse SI) or polarity of the discharge (positive + or negative -).

Calculations were made for the long sparks represented as a set of interconnected segments and not a set of pixels. This eliminated the influence of the method of recording the long spark images (the quality of the photos taken affecting the channel thickness, e.g., the overexposure effect). Thanks to this, the calculated fractal dimension depends solely on the channel shape and thus better reflects the geometry-related features. The input data used in the calculations can be further employed to calculate the tortuosity angles of a discharge without the need to process these data, which may also positively affect the quality of the correlation analysis of the fractal dimension and tortuosity angles. It can also be employed to analyze simulation data since computer simulations provide a spark described as a set of segments.

The measurement results presented in this paper refer exclusively to the described measurement test set-ups. The results suggest that the fractal dimension depends on the type of discharge, its polarity, and the system's geometry. The assessment of the impact of other parameters, such as atmospheric conditions, the overvoltage level stressing the insulation, or impulse chopping time, can be the subject of further research.

The measurement data reported in this paper can serve as an input for modeling work, based on which a simulation model can be developed, involving the statistical nature of voltage breakdowns in long air gaps, which can be utilized in coordination insulation studies. When validated with the measurement data, such a model may be used to analyze various structures of line designs beyond the case-specific laboratory test set-ups reported in this study. Such data are scarce as they require costly experiments to obtain. The data were obtained in a measurement system for large-scale conditions for which it has not been published previously and can serve as input for research groups dealing with modeling and simulations to contribute to developing methods for modeling long sparks for insulation coordination studies.

REFERENCES

- [1] CIGRE Technical Brochure, "Insulation Coordination for UHV AC Systems," Study Committee: C4, WG (TF): WG C4.306, 2013.
- [2] J. Guo et al., "Validation of the Lightning Fractal Model Based on the Attachment Probability Experiments Using Rod-Rod Air Gaps," *IEEE Trans. Power Delivery* 6/37, 2022; doi: [10.1109/TPWRD.2022.3171598](https://doi.org/10.1109/TPWRD.2022.3171598)
- [3] J. Guo et al., "A three-dimensional direct lightning strike model for lightning protection of the substation," *IET Generation, Transmission & Distribution*, 28 May 2021; doi: doi.org/10.1049/gtd2.12213
- [4] Ioannidis, Alexios I., and Thomas E. Tsovilis. "Fractal-based approach for evaluating the shielding design of high voltage substations against direct lightning strikes." 2020 IEEE Industry Applications Society Annual Meeting. IEEE, 2020.
- [5] Ioannidis, Alexios I., and Thomas E. Tsovilis. "Shielding failure of high-voltage substations: A fractal-based approach for negative and positive lightning." *IEEE Transactions on Industry Applications* 57.3 (2021).
- [6] Bian, Xiaoyan, et al. "Quantitative characteristics of the striking distance to wind turbine blades based on an improved stochastic lightning model." *IET Generation, Transmission & Distribution* (2023).
- [7] Ioannidis, A. I., et al. "Fractal-Based Approach for Modelling Electric Breakdown of Air Gaps: An Application to a 75 cm Positive Rod-Plane Gap." *Proceedings of the 21st International Symposium on High Voltage Engineering: Volume 1*. Springer International Publishing, 2020.
- [8] N Femia, L. Niemeyer, V. Tucci, "Fractal characteristics of electrical discharges: experiments and simulation," 1993 *J. Phys. D: Appl. Phys.* 26 619; doi: doi.org/10.1088/0022-3727/26/4/014
- [9] L. Niemeyer, L. Pietronero, H. J. Wiesmann, "Fractal dimension of dielectric breakdown," *Physical Review Letters*, Vol. 52, No. 12, 19 March 1984; doi: [10.1103/PhysRevLett.52.1033](https://doi.org/10.1103/PhysRevLett.52.1033)

- [10] Z. G. Datsios, A. I. Ioannidis, T. A. Papadopoulos, T. E. Tsovilis, "A Stochastic Model for Evaluating the Lightning Performance of a 400 kV HVDC Overhead Line," *IEEE Trans. Electromagnetic Compatibility*, vol. 63, no. 5, pp. 1433-1443, Oct. 2021; doi: [10.1109/TEMC.2021.3054307](https://doi.org/10.1109/TEMC.2021.3054307)
- [11] W. Yu, Q. Li, J. Zhao, W.H. Siew, "Numerical Simulation of the Lightning Leader Development and Upward Leader Initiation for Rotating Wind Turbine," *Machines* 2022, 10, 115; doi: [10.3390/machines10020115](https://doi.org/10.3390/machines10020115)
- [12] A. A. Tsonis, "A Fractal Study of Dielectric Breakdown in the Atmosphere," In: Schertzer, D., Lovejoy, S. (eds) *Non-Linear Variability in Geophysics*. Springer, Dordrecht; doi: [10.1007/978-94-009-2147-4_11](https://doi.org/10.1007/978-94-009-2147-4_11)
- [13] Wan Hao-jiang, Wei Guang-hui and Chen Qiang, "Estimation on lightning protection performance using a fractal approach," *International Conference on Computer Design and Applications*, 2010, pp. V4-339-V4-343; doi: [10.1109/ICCCA.2010.5541095](https://doi.org/10.1109/ICCCA.2010.5541095)
- [14] D. Amarasinghe, U. Sonnadara, M. Berg, V. Cooray, "Fractal dimension of long electrical discharges," *Journal of Electrostatics*, Vol. 73, 2015, pp. 33-37; doi: [10.1016/j.elstat.2014.10.015](https://doi.org/10.1016/j.elstat.2014.10.015)
- [15] S.P.A. Vayanganie, T.A.L.N. Gunasekara, M. Fernando, U. Sonnadara, V. Cooray, M. Rahman, P. Hettiarachchi, O. Diaz, "Fractal Analysis of Long Laboratory Sparks of high Speed Video Recordings," *International Conference on Lightning Protection (ICLP)*, 25-30 Sep. 2016, Estoril, Portugal
- [16] S. Buczkowski, P. Hildgen, L. Cartilier, "Measurements of fractal dimension by box-counting: a critical analysis of data scatter," *Physica A: Statistical Mechanics and its Applications*, Vol. 252, Issues 1-2, 1998, pp. 23-34; doi: [10.1016/S0378-4371\(97\)00581-5](https://doi.org/10.1016/S0378-4371(97)00581-5)
- [17] IEC Std. 60071-1: 2019, *Insulation co-ordination - Part 1: Definitions, principles and rules*.
- [18] IEC Std. 60060-1:2010. *High-Voltage Test Techniques—Part 1: General Definitions and Test Requirements*, ed. 3.0, 2010
- [19] Molas, M.; Szewczyk, M. Experimental Evaluation of 3D Tortuosity of Long Laboratory Spark Trajectory for Sphere-Sphere and Sphere-Plane Discharges under Lightning and Switching Impulse Voltages. *Energies* 2021, 14, 7409. <https://doi.org/10.3390/en14217409>.
- [20] A. Golly, J.M. Turowski, "Deriving principal channel metrics from bank and long-profile geometry with the R package cmgo," *Earth Surface Dynamics* 5.3 (2017): 557-570.
- [21] E. Lewandowicz, P. Flisek. "A Method for Generating the Centerline of an Elongated Polygon on the Example of a Watercourse," *ISPRS International Journal of Geo-Information* 9.5 (2020): 304.
- [22] O. Diaz, "Experimental study of leader tortuosity and velocity in long rod-plane air discharges," *IEEE Trans. Dielectrics and Electrical Insulation* 23.2 (2016): 806-812.
- [23] S. Gu et al., "3D Channel tortuosity of long air gap discharge," 2011 7th Asia-Pacific International Conference on Lightning. IEEE, 2011.

Michał Molas received B.Sc. and M.Sc. degrees in electrical engineering from Warsaw University of Technology in 2012 and 2013 respectively. Since 2013, he has been working at the High Voltage Laboratory of the Institute of Power Engineering in Warsaw (Poland). In 2019, he became the technical head of the High Voltage Laboratory. Currently he is a Ph.D. candidate in Electrical Engineering, with his research focused on methods of measuring and simulating long spark discharges. ORCID: 0000-0001-5954-8335

Marcin Szewczyk (M'12–SM'14) received his M.Sc., Ph.D., and D.Sc. degrees from Warsaw University of Technology, Poland, in 2000, 2009 and 2018 respectively. In 2010-2017 he was with ABB Corporate Research as Principal Scientist and Project Manager of R&D projects in power products and power systems sector. Currently he is Professor at Warsaw University of Technology. His current focus is to establish partnerships towards R&D projects in collaboration between industry and academia partners. Senior Member of IEEE, Member of CIGRE. ORCID: 0000-0003-3699-5559, ResearcherID: A-3936-201